J. Fluid Mech. (1998), *vol.* 371, *pp.* 81–107 Printed in the United Kingdom

Observations of coagulation in isotropic turbulence

By BRETT K. BRUNK[1], DONALD L. KOCH[1]† AND LEONARD W. LION[2]

[1] School of Chemical Engineering, Cornell University, Ithaca, NY 14853, USA

[2] School of Civil and Environmental Engineering, Cornell University, Ithaca, NY 14853, USA

(Received 18 April 1997 and in revised form 7 May 1998)

Turbulent-shear-induced coagulation of monodisperse particles was examined experimentally in the nearly isotropic, spatially decaying turbulence generated by an oscillating grid. The 3.9 μm polystyrene microspheres used in the experiments were made neutrally buoyant and unstable by suspending them in a density-matched saline solution. In this way, particle settling, double-layer repulsion and particle inertia were negligible and the effect of turbulent shear was isolated. The coagulation rate was measured by monitoring the loss of singlet particles as a function of time and reactor turbulence intensity. By restricting consideration to experimental conditions where the singlet concentration was in excess, the effect of higher-order aggregate (i.e. triplet) formation was negligible and nonlinear regression using an integral rate expression that included terms for doublet formation and breakup was used to obtain the turbulent coagulation rate constant. The strength of the van der Waals attractions was characterized with the Hamaker constant obtained from Brownian coagulation experiments. Since particle bulk mixing was fast compared to the coagulation rate, the observed coagulation rate constants were averages over the local coagulation rates within the grid-stirred reactor. Knowledge of the spatial variation of turbulence within the reactor was necessary for quantitative prediction of the experiments because model predictions for the coagulation rate are nonlinear functions of shear rate. The investigation was conducted with particles smaller than the length scales of turbulence and since the smallest turbulent length scales, the Kolmogorov scales, have the highest shear rate they controlled the rate of particle aggregation. The distribution of the Kolmogorov shear rate at various grid oscillation frequencies was obtained by measuring the turbulent kinetic energy (E) using acoustic Doppler velocimetry and relating E to the Kolmogorov shear rate using scaling arguments. The experimentally measured turbulent coagulation rate constants were significantly lower than theoretical predictions that neglect interparticle interactions; however, simulations that included particle interactions showed excellent agreement with the experimental results. The favourable comparison provides evidence that the computer simulations capture the important physics of turbulent coagulation. That is, particle transport on length scales comparable to the particle radius controls the rate of turbulent shear coagulation and particle interactions are significant.

1. Introduction

Turbulence-induced coagulation is an important process leading to the aggregation of colloidal particles in both industrial and environmental processes (McCave 1984). Turbulent mixing is heavily employed in the water treatment and chemical industries

† Author to whom correspondence should be addressed. email: don@cheme.cornell.edu.

to enhance the aggregation and removal of fine particles (Appiah & O'Melia 1990). In natural aquatic systems, pollutants tend to associate strongly with particles and hence considerable effort has been focused on understanding the dynamics of particles in natural environments (O'Melia 1980). In estuaries, for instance, contaminated suspended particles in river water mix with sea water resulting in colloidal destabilization, aggregation, particle settling, and the accumulation of contaminated sediments onto the estuarine benthos (Stumm & Morgan 1981).

Despite the importance of turbulent coagulation, fundamental understanding of the processes leading to coagulation in turbulence is limited. Over the past 40 years a variety of turbulent coagulation models have been proposed (Saffman & Turner 1956; Brunk, Koch & Lion 1997, 1998; Delichatsios & Probstein 1975; Camp & Stein 1943; Casson & Lawler 1990), yet without well-controlled experiments that satisfy the assumptions of the various models, choosing between the theoretical paradigms is problematic. Surprisingly, only a few experimental studies have been undertaken that attempt to meet the hypotheses made in the model calculations. For experimental coagulation rate measurements to be compared reliably with theoretical predictions, the experimental system must generate well-defined nearly isotropic turbulence, the initial particles (singlets) must be monodisperse, only the initial rate of flocculation should be considered so that particle breakup and the formation of higher-order aggregates are negligible, and the system should be dilute so binary collisions dominate the aggregation process (Brunk *et al*. 1997). We shall see below that few, if any, of the existing experimental studies meet these assumptions.

In the environmental engineering literature, jar tests are often used to obtain a qualitative understanding of how the coagulation rate is affected by stirring rate or turbulence intensity (Stumm & Morgan 1981). Delichatsios & Probstein (1975) have correctly noted that the experimental conditions for jar tests are far from ideal because the highly inhomogeneous turbulence created in these systems violates key assumptions of existing turbulence models. As an alternative, Delichatsios & Probstein studied turbulent coagulation in pipe flow. Because turbulence in pipe flow is well understood, it was hoped that these experiments could be used to distinguish between alternative model formulations for the coagulation rate constant. Pipe flow experiments have two main disadvantages: (i) measurement time is limited by the length of pipe used and (ii) large velocity gradients caused by mean flows can significantly affect the reported coagulation rate (Clark 1985). Results from the experiments of Delichatsios & Probstein (1975) agreed with their empirical coagulation model. The model, however, was derived by analogy with the kinetic theory of gas, it did not consider the effects of particle–particle interactions such as van der Waals attraction, and it ignored spatial and temporal distributions of the turbulence intensity. Instead, the work used an empirical estimate for the Kolmogorov shear rate in the turbulent core of the pipe. As is demonstrated in this paper (see §5), both the spatial distribution of turbulence and interparticle interactions can have a considerable influence on the interpretation of experimental data. Hydrodynamic interactions between particles decrease the coagulation rate significantly because of viscous resistance to particle collision. Moreover, in the presence of particle interactions, the coagulation rate is a nonlinear function of the turbulent shear rate (Brunk *et al*. 1998) and so it is inappropriate to use an average shear rate to characterize the turbulent coagulation rate. Rather, it is important to know the detailed spatial distribution of the mean turbulent shear rate to compute the observed rate of coagulation.

Use of an oscillating grid is another option for generating well-characterized turbulence (Hopfinger & Toly 1976; Brumley & Jirka 1987). Casson & Lawler (1991)

reported on coagulation experiments conducted in a grid-stirred apparatus; however, they did not account for turbulence intensity decay with distance from the operating grids. In addition, these investigators used colloidal particles that had a broad particle size distribution, and they reported flocculation rates over long times during which aggregates larger than doublets formed. At long times and for broad particle size distributions, coagulation between multi-particle aggregates can be significant, and the measured coagulation rate does not pertain to the singlet aggregation reaction. Since most coagulation models treat particle aggregates as if they were spherical particles with a volume equal to the total volume of the singlet particles in the floc, these models cannot be expected to be quantitative at large times since the coalescence formulation inaccurately represents the shape of the larger aggregates (Elimelech *et al.* 1995).

In this work, the turbulent shear coagulation rate was measured for monodisperse polystyrene latex particles in turbulence generated by a grid-stirred apparatus. In §2 we briefly summarize the kinetic theory of coagulation and use dimensional analysis to derive the form of the coagulation rate constant. Pertinent results from a computer simulation of turbulent coagulation presented in a companion paper (Brunk *et al.* 1998) are also reviewed briefly in §2. Section 3 describes the general experimental procedures and data analysis techniques used in the coagulation experiments reported in this manuscript. Measurements were made of the initial coagulation rate of monodisperse polystyrene latex particles by monitoring the disappearance of singlet particles and correcting the data for particle breakup. A necessary input for the computer simulation is the Hamaker constant which characterizes the magnitude of the van der Waals attractive potential between the coagulating particles. Brownian coagulation experiments described in §4 were used to estimate the Hamaker constant. The turbulent coagulation experiments were conducted in the locally homogeneous, isotropic turbulence created by an oscillating grid. Turbulence intensities in grid-generated turbulence decay with distance from the grid. Because bulk mixing is fast compared with coagulation, the coagulating particles will experience a spatially varying turbulence field over the course of an experiment. For quantitative comparison between the computer simulations and the experiments, knowledge of the spatial distribution of turbulence within the reactor is necessary. Determination of the turbulence intensity distribution within the grid-stirred reactor is described in §5.2 and related through scaling arguments to the spatial distribution of the Kolmogorov shear rate. Coagulation rates of destabilized particles are presented in §5.3 as a function of the average Kolmogorov shear rate in the reactor. The measured coagulation rates are compared with results obtained from the dynamical simulations of coagulating particles that are smaller than the scales of turbulence (§5.4).

2. Review of turbulent coagulation theory

2.1. *Kinetic rate expression for turbulence*

We restrict the investigation to the initial rate of doublet formation in a dilute suspension of monodisperse spherical particles. Consequently, the loss of singlets in the system is due only to the formation of doublets and the kinetic rate expression is second order in the singlet concentration:

$$\frac{1}{2}\frac{\mathrm{d}S}{\mathrm{d}t} = -kS^2, \tag{2.1}$$

where S is the number concentration of singlet particles and k is the coagulation rate constant. The rate constant incorporates both the transport mechanisms leading to

coagulation (e.g. turbulent shear, Brownian motion and differential settling) and the effect of interparticle interactions (e.g. van der Waals attraction and hydrodynamics). Generally, the coagulation rate constant is decomposed into the product of an ideal rate constant, k^0, that includes the effect of non-interacting particle transport, and a collision efficiency, α, that incorporates hydrodynamic interactions (i.e. viscous drag and lubrication forces) and physicochemical interactions (i.e. van der Waals attraction and electrostatic double layer repulsion). The collision efficiency is defined as the ratio of the coagulation rate obtained when particle interactions are considered to the ideal coagulation rate without particle interactions. Usually, the collision efficiency is less than one, indicating that only a fraction of the collisions occurring for non-interacting particles actually transpire when particle interactions are included in the analysis. Theoretical and empirical expressions for k^0 are available (see Pearson, Valioulis & List, 1984 for a table of ideal rate constants for a variety of particle transport mechanisms); however the collision efficiency must usually be obtained through numerical integration or dynamic simulations.

In turbulence, colloidal particles are typically orders of magnitude smaller than the length scales of turbulence. Since the rate of strain increases with decreasing turbulence length scale (Tennekes & Lumley 1972), the small scales of turbulence (the Kolmogorov scales) dominate the relative motion of neighbouring particles and thus the rate of aggregation. The magnitude of the Kolmogorov scales can be estimated from scaling arguments that balance the turbulent energy flux with the characteristic viscous dissipation. The results are the Kolmogorov scales of length, η, and velocity gradient, Γ:

$$\eta = (\nu^3/\epsilon)^{1/4}, \tag{2.2}$$

$$\Gamma = (\epsilon/\nu)^{1/2}, \tag{2.3}$$

where ϵ is the turbulent dissipation rate and ν is the kinematic viscosity used to parameterize the effects of viscosity. Direct numerical simulations (DNS) indicate that the turbulent velocity gradient experienced by a fluid particle is controlled by two correlation time scales: τ_S and τ_R for the strain and rotational components of the flow, respectively (Girimaji & Pope 1990). Numerical integration of strain and rotation rate correlation functions taken from DNS (Girimaji & Pope 1990) indicates that $\tau_S \Gamma \approx 2.3$ and $\tau_R \Gamma \approx 7.2$ (Brunk *et al.* 1997*b*).

Dimensional analysis can be used to ascertain the functional form of the turbulent shear coagulation rate constant. Since any directional information imposed at large scales of turbulence will be lost during the energy cascade process, we assume isotropy and homogeneity at the small scales of turbulence and therefore the only length scale affecting the coagulation rate constant of monodisperse particles will be their radius, a. For sufficiently large separation of the colloidal and turbulence length scales, $a \ll \eta$, the flow field in the neighbourhood of two coagulating particles may be assumed to be approximately linear and can be characterized by the velocity gradient. If we ignore particle inertia then the flow field provides the only time scales in the scaling analysis. Representing the fluctuating velocity gradient with its magnitude and correlation time yields the expectation that $k_T = f(\Gamma, \tau_S, \tau_R, a)$ or, after combining into non-dimensional groups:

$$k_T = \alpha_T \beta(\tau_S \Gamma, \tau_R \Gamma)\, \Gamma a^3, \tag{2.4}$$

where the subscript T denotes that this is the turbulent shear coagulation rate constant, a is the radius of a singlet particle, α_T is the collision efficiency that accounts for the effect of interparticle interactions. The function $\beta(\tau_S, \Gamma, \tau_R \Gamma)$ accounts for the

kinematics of the flow field and it is made explicit in several turbulent coagulation models (Saffman & Turner 1956; Brunk *et al*. 1997, 1998; Delichatsios & Probstein 1975; Camp & Stein 1943). For large total strain and rotation, particle coagulation occurs in a pseudo-steady flow field and β becomes independent of the flow time scales. In the limit of small total strain, particle transport is diffusive leading to a β that is proportional to the total strain (Brunk *et al*. 1997).

The effect of rotation on the rate of coagulation is not immediately obvious. In Brunk *et al*. (1998) we show that rotation can reduce coagulation rates; we propose that rotation leads to the formation of looped trajectories that leave and return to the potential collision site. These closed trajectories will not lead to collisions. Therefore, the rate of coagulation will be lower than that seen in an irrotational flow.

2.2. *Review of turbulent coagulation dynamical simulations*

In a companion paper (Brunk *et al*. 1998), computer simulations of interacting particles in Gaussian isotropic turbulence are used to estimate the turbulent coagulation rate constant in the presence and absence of hydrodynamic interactions and van der Waals attractions. Below, salient results are extracted for comparison with the experimental measurements of turbulent coagulation.

Analytical predictions for turbulent-shear-induced coagulation have been derived for the large and small total strain limits. The total strain can be conceptualized as a measure of the total amplitude of the temporally varying flow and it is defined as the product of the characteristic strain rate and its correlation time (i.e. $\Gamma\tau_S$). The well-known turbulent coagulation model derived by Saffman & Turner (1956) applies for irrotational flows in the large total strain limit where the velocity field is persistent, while the present authors have recently investigated coagulation in the small strain limit (Brunk *et al*. 1997), where the rapidly fluctuating velocity field causes diffusive transport. DNS investigations of Lagrangian statistics in isotropic turbulence have indicated that the total strain is order one (Pope 1990; Girimaji & Pope 1990) bringing into question the applicability of both previously derived asymptotic limits to turbulent coagulation.

In the numerical simulations, trajectory calculations of turbulent coagulation at arbitrary total strain were used to predict the actual coagulation rate and to compare with the large and small total strain asymptotic limits (Brunk *et al*. 1998). For particles smaller than the length scales of turbulence, the relative motion of particles was represented as a temporally varying linear flow field. The fluctuating velocity gradient was assumed to be isotropic and Gaussian with two-time Lagrangian statistics taken from DNS (Girimaji & Pope 1990). Coagulation rates were obtained in the presence and absence of hydrodynamic interactions and van der Waals attractions. The reader is referred to Brunk *et al*. (1998) for complete details on the simulation procedure and an interpretation of the results.

In the absence of particle–particle interactions the turbulent coagulation rate constant depends on the total strain and total rotation in the system. Simulations based on the correlation times $\tau_S\Gamma_\eta = 2.3$ and $\tau_R\Gamma_\eta = 7.2$, obtained from DNS calculations in isotropic turbulence (see Brunk *et al*. 1998), indicate that $\beta = 8.62 \pm 0.02$, so that

$$k_T = 8.62\alpha_T\Gamma a^3. \tag{2.5}$$

The collision efficiency, α_T, has been calculated for non-Brownian particles experiencing hydrodynamic interactions and retarded van der Waals attraction. When van der Waals attractions and hydrodynamic interactions are included, two additional

non-dimensional parameters govern the behaviour of the system. $N_L = 4\pi a/\lambda_L$ is the ratio of the particle size to the London retardation wavelength, λ_L. The retardation wavelength characterizes the distance at which van der Waals attractions are reduced because of the finite propagation speed of electromagnetic radiation between atoms on neighbouring particles (Russel, Saville & Schowalter 1989). The shear number, $N_S = 12\pi\mu a^3\Gamma/A_H$, describes the relative importance of the viscous and van der Waals forces. Here, μ is the fluid viscosity and A_H is the Hamaker constant.

Coagulation rates in isotropic turbulence were computed for several values of N_L and N_S. When $N_L > 10$, the collision efficiencies simulated for the 3.9 μm diameter particles used in this research could be represented ($r^2 = 97\,\%$ where r^2 is the coefficient of determination) with the following power law:

$$\alpha_T = 0.56 N_S^{-0.16}. \tag{2.6}$$

This result implies that, in the presence of particle interactions, the coagulation rate constant increases in proportion to $\Gamma^{0.84}$.

3. Coagulation experiments

Below, experimental protocols used to measure the singlet concentration evolution in a coagulating suspension are described. Subsequently, the data analysis technique used to extract the coagulation rate constant from the rate of singlet particle depletion is presented.

3.1. *Experimental procedure*

Monodisperse sulphate polystyrene latex particles (Interfacial Dynamics Corp., OR) having a density of 1.055 g cm^{-3} were used as the coagulating particles for the experiments. Using a Coulter Multisizer II (Coulter Corp., FL), the number-averaged particle diameter was measured to be 3.9 μm with a ± 0.3 μm standard deviation indicating that the microspheres were nearly monodisperse. The particles were stored at 4 °C in distilled water before use. During coagulation experiments, a density-matched saline solution, created by adding 75.6 g l^{-1} NaCl to distilled water, was used to suspend the latex particles and to eliminate the effects of double-layer repulsion between particles.

Coagulated samples were stored for analysis in a density-matched, glucose-based storage solution made by adding 6.5 g l^{-1} NaCl, 2.5 g l^{-1} NaN_3 and 137 g l^{-1} glucose to distilled water. The glucose was added to increase the solution density to within 1 % of the bead density, NaCl was used as a background electrolyte and NaN_3 was used to inhibit bacterial growth in the storage solution. All storage solutions were pre-filtered through 0.4 μm membrane filters to remove background particulates.

Density matching was important because it prevented particles from settling out of suspension during and after an experiment and it reduced gravity- and turbulent-acceleration-induced coagulation of different size particles. The density difference between the particles and the solution was always less than 0.01 g cm^{-3}. For this maximum density difference the calculated particle settling velocity was insignificant compared to the turbulent integral scale velocities measured in the experiments. Similarly, using estimates from Saffman & Turner (1956), coagulation due to turbulent acceleration was predicted to be unimportant compared to turbulent shear for the experimental conditions reported in this manuscript (see §5). The coagulation rate constant for differential settling of a singlet and a doublet particle was at least five times smaller than the turbulent shear and Brownian coagulation rate constants when

coagulation kernels summarized by Pearson *et al.* (1984) were used. Since the rate of differential settling coagulation depends on the concentration of doublets in the system, it was inconsequential as long as our experiments contained few doublets. Therefore, using density-matched solutions and analysing only data for which there were excess singlets ensured that turbulent shear controlled the observed particle motion and coagulation.

During an experiment, aliquots of coagulating suspension were periodically withdrawn and diluted in particle-free plastic vials containing the density-matched glucose-based storage solution. The particle size distributions of the diluted samples were measured within 1 h. Preliminary experiments showed that coagulated particles could be stored longer than 6 h without significant alteration of the observed particle size distribution and concentration. Samples were measured using the Coulter Multisizer with a 100 μm aperture. The instrument measures changes in conductivity that occur as particles are transported through the aperture. The magnitude and duration of the conductivity spikes are related to the volume of the particle passing through the aperture. Particle volumes are converted into particle diameters assuming spherical particles.

There are three significant analytical concerns associated with the Coulter Multisizer. First, the concentration of particles in the suspension must be low enough so that the probability of measuring two particles simultaneously, termed the coincidence, is small. By diluting samples to contain about 10000 particles/ml, coincidence was kept to less than 2% of the sample population. Secondly, the statistical uncertainty in the concentration caused by counting a finite number of particles was reduced by measuring at least 20000 particles for each sample. Finally, since the maximum shear rates at the aperture are large (the shear rate at the wall is greater than 10^5 s^{-1} for the apertures used in this analysis) control experiments were required to ensure doublet breakup near the aperture opening did not skew the measurements (Gibbs 1982). To test for the effects of doublet breakage, coagulation experiments were analysed using 30, 100 and 140 μm diameter apertures. The particle concentrations measured with the three apertures agreed to within 10% indicating that each aperture was sampling the particle suspension similarly despite the 10-fold variation in the wall shear rate over the 30 to 140 μm aperture size range. It is possible that doublets actually broke up near the aperture, but did not separate sufficiently to be counted as separate particles by the device. This experimental evidence indicates that aggregate breakup in the Coulter Multisizer II did not influence the measured doublet concentration.

Figure 1 shows an example of the raw output from the Coulter Multisizer at the beginning (dashed line) and end (solid line) of a coagulation experiment. The emergence of a distinct doublet peak indicates that flocculation was occurring and could be accurately measured with the instrument.

Calculation of the initial coagulation rate constant from the experimental particle size distribution data depends on knowing the ratio of the singlet concentration to its initial value rather than the absolute singlet concentration (see discussion below). The number concentration in the diameter interval from 3.0 to 3.9 μm (designated with the vertical dotted lines on figure 1) was used as a measure of the singlet concentration. By choosing this size interval we measure about half of the singlet concentration distribution. Since we measure the lower half of the size distribution, the error caused by counting unusually small doublet particles (created by the aggregation of two smaller than average singlet particles) as singlets is significantly reduced.

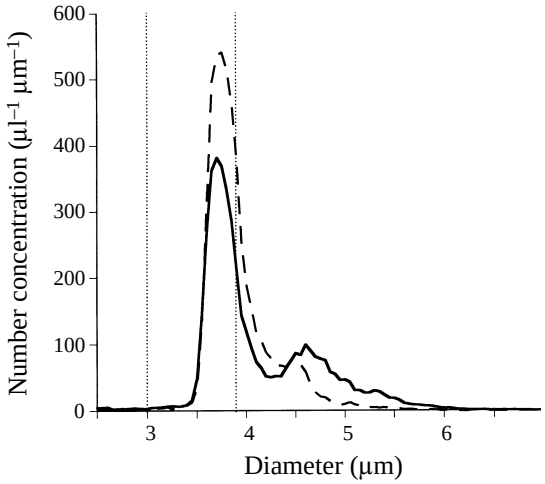

FIGURE 1. Typical particle size distributions obtained at the beginning (dashed line) and end (solid line) of a coagulation experiment. The final results show the formation of a significant doublet peak compared to the initial particle size distribution, indicating coagulation of the singlet particles. Dotted lines bracket the region of particle size distribution used as a measure of the singlet concentration.

3.2. *Coagulation rate constant determination*

If the concentration of singlet particles is in excess, (2.1) can be rewritten as a pseudo-first-order expression depending on the particle volume fraction:

$$\frac{\mathrm{d}S}{\mathrm{d}t} = -k'S, \tag{3.1}$$

where $k' = (3\phi/2\pi a^3)\ k$ and ϕ is the volume fraction of particles. The use of the pseudo-first-order approximation requires $S/(S_0 - S) \quad 1$, where S_0 is the initial concentration of singlet particles. The linearized expression given by (3.1) has the advantage of leading to an integral rate expression that depends on the relative concentration of singlet particles (see equation (3.2)). As noted above, the relative concentration of singlets was estimated from the experimental data rather than the absolute singlet concentration since the relative concentration could be determined more accurately.

In a closed system, the particle volume fraction is a constant and (3.1) can be integrated subject to the initial condition that when $t = 0$, $S = S_0$:

$$\ln(S/S_0) = -k't. \tag{3.2}$$

A plot of $\ln(S/S_0)$ against time should yield a straight line with the slope being proportional to the rate constant, k'.

Since the above rate expression is predicated on doublet formation being the only coagulation process occurring, data collection must stop once the formation of larger-order aggregates becomes significant. Aggregates made by the collision of a doublet and a singlet (i.e. a triplet) are most likely to form next. A simple estimate for the importance of triplet formation can be obtained by taking the ratio of the doublet to triplet coagulation rates. Denoting doublet concentration with D and triplet concentration with T, this ratio is given by

$$\frac{\mathrm{d}D/\mathrm{d}t}{\mathrm{d}T/\mathrm{d}t} = \frac{\alpha k^0 S^2}{\alpha_3 k_3^0 SD}, \tag{3.3}$$

where the numerical subscripts indicate the number of primary particles in the aggregate. If α and k^0 are not strong functions of aggregate size, (3.3) reduces to

$$\frac{\mathrm{d}D/\mathrm{d}t}{\mathrm{d}T/\mathrm{d}t} \approx 2\frac{S}{S_0 - S}, \tag{3.4}$$

where a particle balance was used to relate D to S, assuming the concentration of higher-order aggregates is negligible, i.e. $D = 1/2(S_0 - S)$. To within an order-one constant, this is the same criterion that must be met to use the pseudo-first-order approximation in (3.1).

Aggregate breakup can also alter the rate of singlet depletion. Breakup is characterized by a decrease in the observed coagulation rate until the system reaches steady state. In other words, at steady state the formation of doublets is balanced by breakup of doublets and the effective coagulation rate becomes equal to zero. In the following investigations aggregate breakup was significant at the higher turbulent shear rates. Doublet breakup was modelled explicitly by including a term in the rate equation for the singlet concentration dependent on the doublet concentration. Thus, (3.1) becomes

$$\frac{\mathrm{d}S}{\mathrm{d}t} = -k'_T S + 2bD, \tag{3.5}$$

where b is the unknown doublet breakup rate constant that is conjectured to depend on the turbulence intensity (McCave 1984). After substituting $D = 1/2(S_0 - S)$ for the doublet concentration, (3.5) can be integrated to obtain

$$\frac{S}{S_0} = \frac{b + k'_T \exp\left[-(b + k'_T)\, t\right]}{b + k'_T}. \tag{3.6}$$

When breakup is included, the singlet concentration approaches a non-zero value at long times: $S/S_0 = b/(b + k'_T)$ when $t \to \infty$. In cases where a horizontal asymptote in the singlet concentration was experimentally observed, nonlinear regression of the experimental data using (3.6) was used to estimate the coagulation rate constant and the breakup rate constant. The highest shear rate experimental data was difficult for our nonlinear regression routine to resolve because of the rapid transition from doublet formation to steady state which caused the regression routine to be very sensitive to initial conditions. We found that nonlinear regression for the high shear rate routinely converged on solutions representing local rather than global minima of the error. Fortunately, the abrupt transition to steady state made it easy for us to identify when breakup began to become important in these experiments. For this reason, we chose to linearize the experimental data at the highest shear rate using the model without breakup (3.2) and do a linear regression on the experimental data. For this to work we had to decide when breakup was significant so that the data contaminated by breakup could be neglected. We did this by monitoring the r^2 and standard errors of the regression coefficients as the number of data points included in the regressed increased. The fit improved as we added initial rate data and the fit became worse when breakup contaminated the measurements. The linear regression with the smallest errors was used to estimate doublet formation.

4. Estimation of the Hamaker constant

The Hamaker constant (A_H) provides a measure of the strength of the van der Waals attraction between colloidal particles. It was necessary to estimate its value for the

3.9 μm diameter polystyrene beads used in these experiments before the turbulent coagulation experiment and simulation results could be compared. Previous experimental estimates for A_H obtained from Brownian coagulation experiments range from $0.7k_b T$ to $1.9k_b T$ for polystyrene particles (Russel *et al.* 1989), where k_b is the Boltzmann constant and T is the absolute temperature. Most of the variation in the estimated Hamaker constants is attributed to the weak dependence of the Brownian collision efficiency on the Hamaker constant (Russel *et al.* 1989).

The Hamaker constant was obtained by fitting theoretical predictions for the Brownian coagulation rate constant to experimental data. Besides providing an estimate for A_H, agreement of the experimentally determined value of A_H with previous estimates furnished evidence that the extent of coagulation measured with the Coulter Multisizer was reasonable.

4.1. *Data analysis and procedure*

The initial rate of Brownian coagulation is second order in the singlet concentration and its kinetic expression is given by (2.1), where $k = k_B = \alpha_B 8k_b T/3\mu$ is the Brownian diffusion coagulation kernel (Russel *et al.* 1989) and α_B is the Brownian coagulation collision efficiency incorporating the effects particle interactions.

The Brownian coagulation collision efficiency has been computed for particles influenced by hydrodynamic interactions, van der Waals attraction and electrostatic double-layer repulsion (Spielman 1970; Valioulis & List 1984). Spielman (1970) considered Brownian coagulation for particles influenced by a non-retarded van der Waals potential, while Valioulis & List (1984) extended the calculations to include the effects of van der Waals retardation. Unfortunately, numerical results were only provided for particles smaller than 1 μm diameter.

The equation for α_B can be derived from the steady-state radial pair diffusion equation valid for a particle influenced by Brownian motion, hydrodynamic interactions and an interparticle potential. In agreement with others (Russel *et al.* 1989; Spielman 1970; Valioulis & List 1984) the following result was obtained for equal sized particles:

$$\frac{1}{\alpha_B} = 2\int_2^\infty \frac{\exp(\Phi/k_b T)}{G(r)}\frac{\mathrm{d}s}{s^2}, \tag{4.1}$$

where Φ is the interparticle potential, $s = r/a$ is the particle separation distance scaled by the particle radius and $G(r)$ is the radial relative mobility for two hydrodynamically interacting Brownian particles (Batchelor 1976). The solution of (4.1) was obtained using a fifth-order Runge–Kutta algorithm with adaptive step control (Press *et al.* 1992). The van der Waals potential reported by Schenkel & Kitchener (1960) was used for Φ and values of $G(r)$ were taken from Kim & Karilla (1991). Additional details on the integration method and the form of Φ may be found in Brunk *et al.* (1997). In figure 2 the solid line shows the model prediction for the Brownian coagulation collision efficiency versus A_H/kT.

Brownian coagulation experiments were conducted in the density-matched saline solution. Double-layer interactions were assumed to be negligible due to the high ionic strength of the suspending medium, so only hydrodynamic interactions and van der Waals forces affected the experimentally determined Brownian coagulation rate.

The coagulation rate was calculated by the methods outlined in §3. In the Brownian coagulation experiments doublet breakup was not important so the integral rate expression given by (3.2) was used in the data analysis. Experiments were conducted in particle-free plastic vials containing approximately 22 ml of solution. A reaction

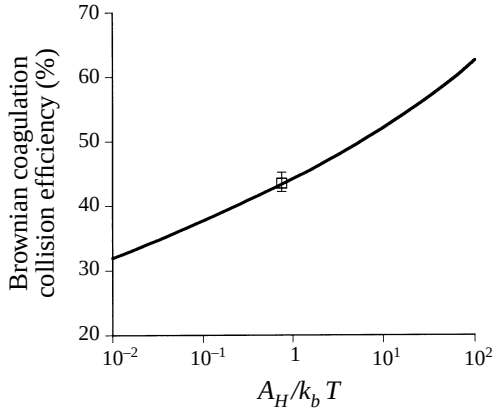

FIGURE 2. Model predictions for the Brownian coagulation collision efficiency against the Hamaker constant for 3.9 μm diameter monodisperse polystyrene spherical particles. The square represents the experimentally determined α_B for the 3.9 μm latex particles used in this manuscript. Error bars are 60% confidence intervals.

half-life of about 90 min was chosen for the experiments which meant that the initial bead concentration in the vials had to be about 9.5×10^6 particles/ml. Initially, each vial was filled with 2 ml of filtered distilled deionized water. Enough beads were added so that when diluted to 22 ml the vial would contain the correct number concentration of singlets. The 2 ml suspension of beads was placed in a sonicating bath for three minutes to break up any doublets. Then, 20 ml of saline solution was quickly poured into the vial to mix the beads and 'start' Brownian coagulation. Fluid motions caused by pouring were allowed to subside. After waiting 5 min, samples of the suspension were taken every 5 min over 45 min. At each sampling time, 52 μl were removed and diluted 1:400 in previously tared vials containing density-matched glucose solution. Samples were taken using an Eppendorf automatic pipette with the plastic pipette tip enlarged to 1–2 mm diameter. The larger diameter pipette tip was used to minimize particle breakup due to shear caused by sampling (Gibbs 1982).

4.2. *Brownian coagulation experimental results*

For each Brownian coagulation experiment a mass balance was computed as a function of elapsed time. Examination of the volumetric concentration evolution data showed that the system was well mixed and temporal trends caused by particle losses/gains were not apparent.

The evolution of the singlet concentration for a representative experiment is shown in figure 3 along with a best-fit line through the data using (3.2). For this experiment, $k_B = 4.72 \pm 0.28\ \mu m^3\ s^{-1}$ with an r^2 of 94%. Error bars are 95% confidence intervals based on Poisson statistics.

The average Brownian coagulation rate constant was obtained from five independent experiments and the average rate was normalized by the Brownian coagulation rate without interparticle interactions to yield $\alpha_b = 43.7\%$ with 60% confidence intervals of $\pm 1.5\%$. Using this collision efficiency with figure 2 yields an average $A_H/k_b T = 0.75$ shown as the open square on the graph. The collision efficiency is insensitive to the value of the Hamaker constant; thus, the 60% confidence interval of A_H is wide ($0.5k_b T$ to $1.3k_b T$). The best estimate for $A_H/k_b T$, however, compares favourably to estimates summarized in Russel *et al.* (1989).

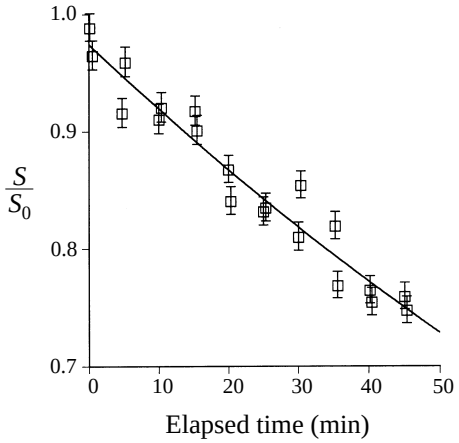

FIGURE 3. Linearized singlet concentration evolution data obtained in a Brownian coagulation experiment. The solid line is a best fit through the experimental data and the error bars are 95% confidence intervals based on Poisson statistics.

5. Turbulent coagulation experimental results

Experimental measurements of the turbulent coagulation rate are presented below and compared with the computer simulations of turbulent coagulation. Experiments were conducted in the spatially decaying, isotropic turbulence created by an oscillating grid device. First, we present the technique for measuring the Kolmogorov shear rate in the reactor. Measurements of the turbulent coagulation rate are then correlated with the spatially averaged Kolmogorov shear rate. Finally, the coagulation rate as a function of average Kolmogorov shear rate in the reactor is compared with the turbulent coagulation model summarized above (see §2). The comparison between simulation and experiment also illustrates the importance of correctly relating the model predictions to the local turbulent conditions of the reactor. Comparison is also made between the computer simulations and the turbulent pipe flow coagulation experiments conducted by Delichatsios & Probstein (1975).

5.1 *Turbulent coagulation materials and methods*

Experiments were conducted in an oscillating grid reactor system that was originally designed to simulate the vertical distribution of turbulence typical for natural aquatic systems. The reactor has been shown to produce well-defined homogeneous, isotropic turbulence that follows established grid-stirred turbulence scaling laws (Brunk *et al.* 1996) and it has been used in stratified flow (Jensen 1997) and sediment transport studies (Brunk *et al.* 1996).

For this work, experiments were conducted with a single oscillating grid in the bottom fifth of the reactor described in previous publications (Brunk *et al.* 1996; Jensen 1997) to minimize the number of polystyrene beads used in a single experiment. The $20 \times 40 \times 25$ cm glass and stainless steel reactor contains a 20×40 cm turbulence-generating stainless steel grid woven from 2.67 mm rods. The mesh spacing is 1.27 cm giving the grid a solidity of 37.6%. The centre of the grid stroke is located 4 cm from the back of the reactor. The grid stroke (twice the oscillation amplitude) can vary from 0.5 to 4 cm and the frequency of oscillation from 0 to 8 Hz. A diagram of the reactor system is shown in figure 4.

The intensity of the turbulence created in the reactor can be varied by changing the

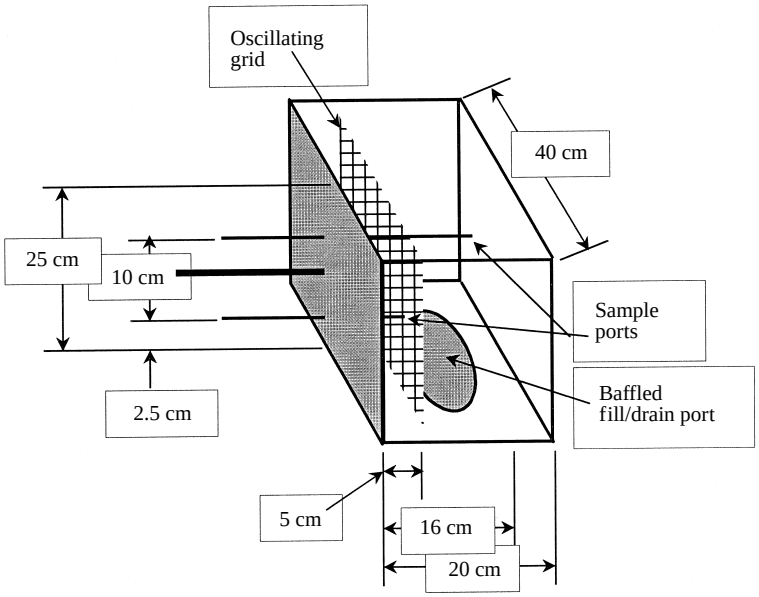

FIGURE 4. Diagram of the bottom of the grid-stirred apparatus used in the turbulent coagulation experiments. The schematic shows the location of sampling ports (5 cm and 16 cm from the back wall of the apparatus) and the dimensions of the coagulation experiment control volume. The centre of the grid stroke is located 4 cm from the back of the reactor.

oscillation frequency and the stroke length of each grid. An acoustic Doppler velocimeter (ADV) was used to measure three components of the turbulent velocity. The velocimeter samples a cylindrical volume 3 mm in radius and 3–9 mm high at a rate of 25 Hz. The sample volume location is 5 cm below the signal transducers to minimize the effect of the probe on the acquired velocity data (Lohrman, Cabrera & Kraus 1994). Additional details about the construction and operation of the grid-stirred reactor may be found in Brunk *et al.* (1996).

The tank was filled with pre-filtered density-matched saline solution through the baffled fill/drain port. For each experiment the reactor contained approximately 20 l of a particle suspension. Samples taken from the reactor before addition of the polystyrene beads indicated that particle contamination was indistinguishable from background noise. After filling with the filtered saline solution, the oscillating grid was set at the desired frequency and the reactor was allowed to reach a hydrodynamic steady state.

Using (2.4) in (3.2) and published values for β and α_T ($\beta \approx 10.4$, $\alpha_T = 1$; Saffman & Turner 1956), the particle concentration needed to obtain a coagulation half-life of 40 min was estimated. For this calculation, the characteristic Kolmogorov shear rate was approximated using the methods outlined below in §5.2. For each turbulent coagulation experiment, the required number of beads was diluted in 100 ml of filtered distilled water and sonicated for several minutes. Afterwards the stock solution was distributed rapidly and equally over the water surface. The system was allowed to mix for 30 s before sampling began. Samples were taken from the two ports shown in figure 4, placed 2.5 cm from the bottom and 5 cm from the back of the reactor and 12.5 cm from the bottom and 16 cm from the back of the reactor. Aliquots of approximately 1 ml were taken from the reactor periodically and placed in previously tared, particle-free vials containing the density-matched glucose diluant.

	Grid frequency (Hz)				
	1	3	4	6	8
$\langle\Gamma\rangle$ (s^{-1})	3.7	19.29	29.6	54.3	83.6
η_{min} (μm)	240	105	85	63	50
$\langle\eta\rangle$ μm)	520	228	184	135	109
Re	71	214	286	428	572
Re_λ	39	67.5	78	95	110
$\langle Pe\rangle$	79	410	632	1162	1789

TABLE 1. Measured and estimated parameters for the oscillating grid turbulence apparatus. $\langle\Gamma\rangle$ is the Kolmogorov shear rate spatially averaged over the grid-stirred reactor. η_{min} is the smallest local Kolmogorov length scale in the grid-stirred reactor. The smallest η will be located in the region of highest turbulence, $-2 < x < 2$ cm. $\langle\eta\rangle$ is the spatially averaged Kolmogorov length scale. $Re = u'l/\nu$ is the turbulent Reynolds number. $Re_\lambda = u'\lambda/\nu$ is the Taylor-scale Reynolds number where $\lambda = 4Re^{1/4}\eta$ is the Taylor scale. $\langle Pe\rangle = \Gamma a^2/D$ is the spatially averaged Péclet number where D is the Brownian diffusivity of the 3.9 μm diameter particles.

5.2. *Characterization of oscillating grid turbulence*

Turbulence generated in an oscillating grid system decays rapidly with distance from the grid (Hopfinger & Toly 1976); thus, coagulating particles will experience a spatially varying distribution of Kolmogorov shear rate as they migrate throughout the reactor. If the system is well-mixed, aggregating particles will sample the entire reactor space during coagulation; therefore, it would be reasonable to expect the observed coagulation rate measured at a single point to be related to the spatial distribution of shear rates (and hence the distribution of local coagulation rates) with the reactor.

In this section, estimates for the Kolmogorov shear rate are provided as a function of the oscillating grid frequency and distance from the grid. The local estimates for Γ are subsequently used to relate the experimental coagulation rate constant to the volumetrically averaged shear rate in the reactor.

The assumption that the reactor is well mixed can be evaluated by comparing the characteristic time for coagulation to the reactor mixing time. An estimate for the characteristic coagulation time is $\tau_c = 1/k'$. A conservative estimate for the reactor mixing time is given by the turbulent diffusion time scale, $\tau_i = H^2/u'L$ where H is the reactor height (25 cm), L is the integral length scale (i.e. the length scale of the largest turbulent eddies) and u' is the root-mean-square velocity. Taking the ratio of τ_c and τ_i and simplifying yields

$$\frac{\tau_c}{\tau_i} \approx \frac{1}{\Phi Re^{1/2}}\left(\frac{L}{H}\right)^2, \tag{5.1}$$

where $u'/L\Gamma \approx Re^{-1/2}$ (Tennekes & Lumley 1972) and $Re = u'L/\nu$ is the turbulent Reynolds number. Measurements of steady-state sediment transport in the experimental apparatus suggest that $H/L \sim 3$ (Brunk *et al.* 1996). The highest particle volume fraction used in the turbulent coagulation experiments was $\Phi = 10^{-5}$, indicating that the Reynolds number would have to be at least 10^8 for the well-mixed assumption to be poor. The turbulent Reynolds numbers generated in the apparatus were considerably lower than 10^8 (see table 1), thus the assumption that the coagulating particles sample the entire reactor was justified.

Comparison between experimental coagulation rates obtained in the oscillating grid reactor and model calculations are predicated on obtaining an accurate estimate for the Kolmogorov shear rate distribution within the reactor. As described above (§2.1), the

Kolmogorov shear rate can be found through scaling arguments by balancing the turbulent dissipation rate, ϵ, with the viscous dissipation to obtain (2.3). The difficulty in using this relation lies in obtaining an accurate estimate for the turbulent dissipation rate. There are two main techniques that can be employed to accomplish this: direct measurement of ϵ and scaling arguments.

The dissipation rate is a small-scale quantity that depends on the mean-square fluctuating velocity gradient tensor (Tennekes & Lumley 1972). Since the power spectrum for the velocity derivative peaks in the dissipation subrange of turbulence (i.e. at Kolmogorov length scales) a direct measurement of ϵ would require a velocity probe with spatial and temporal resolution that is comparable to the Kolmogorov scales (e.g. $\eta \sim 0.5$ mm). The acoustic Doppler velocimeter used in this study had a limited sampling resolution of about 3 mm that was unable to resolve the fine scales of turbulence. For instance, turbulent kinetic energy power spectra obtained with the instrument showed only a small portion of the inertial ranges of turbulence. Consequently, an indirect measure was used for estimating the turbulent dissipation rate.

The turbulent dissipation rate can be related to the turbulent energy input at the large scales by (Tennekes & Lumley 1972).

$$\epsilon \approx \gamma \frac{u'^3}{L}, \tag{5.2}$$

where γ is an order-one constant typically taken to be 0.8 (Townsend 1976). Considerable empirical evidence suggests that this scaling relationship provides a robust estimate for ϵ as long as the turbulence has reached spectral equilibrium (Tennekes & Lumley 1972). Spectral equilibrium implies that all of the local turbulence is dissipated locally. In our reactor, turbulence is created at the grid region and transported to the far field of the reactor. Thus, we would expect that the turbulence in the grid region is not at steady state. Consequently, the dissipation rates measured in the near field may overestimate the actual dissipation rate. In the far field, the turbulence should be closer to equilibrium so our estimates will be more accurate. Without additional experiments using more sophisticated measuring techniques it is not possible to estimate the error in our use of (5.2); however, the reproducibility of our experimental results and their agreement with the computer simulations (see below) suggests that the rate of aggregation is not sensitive to the inhomogeneities of the experimental turbulence.

For convenience, (5.2) is recast in terms of the turbulent kinetic energy (E), where $2E = 3(u')^2$, and substituted into (2.3). After manipulation, an expression relating the Kolmogorov shear rate to the turbulent kinetic energy and the integral length scale is obtained:

$$\Gamma \approx \left[\frac{\gamma(\frac{2}{3}E)^{3/2}}{L\nu}\right]^{1/2}. \tag{5.3}$$

The variation of the integral length scale (L) with distance from the oscillating grid (x) has been investigated previously (Hopfinger & Toly 1976; Brumley & Jirka 1987; E & Hopfinger 1986). Hopfinger & Toly (1976) found that L was proportional to x with the proportionality constant, B, ranging from 0.1 to 0.35 depending on the grid stroke (St) and grid mesh spacing (M). Further investigations by E & Hopfinger (1986) indicated that B is larger for large St/M. The ratio of stroke to mesh size is large in the reactor; therefore, a value of $B = 0.35$ was chosen for this study. In the near field the integral length scale was set at the mesh spacing since this length was expected to

dominate in the oscillating grid region. The integral scale was made a piecewise continuous function of distance from the oscillating grid by setting L to the mesh size, 1.27 cm for $x < 3.63$ cm, and allowing it to vary linearly with distance in the far field ($x > 3.63$ cm).

At distances far from the oscillating grid, the integral scale velocity decays with distance from the oscillating grid and is well represented by the scaling relation developed by Hopfinger & Toly (1976):

$$u'/fS = C_{HT}(S^{1/2}M^{1/2}/x), \tag{5.4}$$

where f is the grid frequency (Hz), St is the grid stroke (4 cm for these experiments), M is the centre-to-centre mesh spacing (1.27 cm for these experiments), x is the horizontal distance from the centre of the operating grid stroke and C_{HT} is a constant found to be about 0.25 (Hopfinger & Toly 1976), although values of C_{HT} ranging from 0.22 to 0.27 (De Silva & Fernando 1992) have been reported. This scaling relationship has been subsequently verified by a number of other researchers (De Silva & Fernando 1992; Brumley & Jirka 1987; Fernando & Long 1985).

The isotropy of grid-generated turbulence may be used to rewrite (5.4) in terms of E (Brunk *et al.* 1996):

$$E = \tfrac{3}{2}C_{HT}^2\frac{f^2St^3M}{x^2}. \tag{5.5}$$

Estimates for the range over which (5.4) and (5.5) are applicable vary from $x > 4St$ (De Silva & Fernando 1992) to $x > 2M$ (Atkinson, Damiani & Harleman 1987). As shown below, the Atkinson *et al.* (1987) estimate of $x > 2M$ held well for the grid parameters used in these experiments.

For this work, the turbulent kinetic energy distribution in the near and far field of the grid were both required to estimate the spatial distribution of Γ using (5.3). To that end, turbulence measurements were made as a function of distance from the oscillating grid. The stroke was held constant at 4 cm and f was varied from 0 to 8 Hz giving turbulent Re as high as 572 for $f = 8$ Hz. The turbulence parameters obtained for the reactor are summarized as a function of oscillating grid frequency in table 1. Three-component velocity data were obtained for different reactor operating conditions using the *in situ* ADV probe (Sontek Inc., CA) at a data rate of 25 Hz for at least 300 s. At each grid frequency, velocity samples were taken at several vertical and horizontal positions in the plane a distance x from the oscillating grid and the velocity data were combined for the ensuing analysis.

The scaling law for E depends only on distances parallel to the grid motion, implying that grid-stirred turbulence is homogeneous in planes perpendicular to the grid motion. This was verified through detailed mappings of the turbulent kinetic energy variation over a plane parallel to an oscillating grid. The E-distributions parallel to the oscillating grid had an absence of long-range structure and a relatively narrow variance relative to the average E (Brunk *et al.* 1996).

For each grid frequency, the turbulent kinetic energy data obtained in the far field (i.e. $x > 2M$) were plotted against the right-hand side of (5.5) to verify the scaling relation in the reactor and obtain an estimate for C_{HT}. The scaling law fit the experimental data with r^2 ranging from 61% to 92% and the predicted C_{HT} varied from 0.22 to 0.24 in agreement with the work of others (Hopfinger & Toly 1976; De Silva & Fernando 1992). In figure 5 the data sets for various grid frequencies are combined and compared with the scaling law using the frequency-averaged value of $C_{HT} = 0.225$.

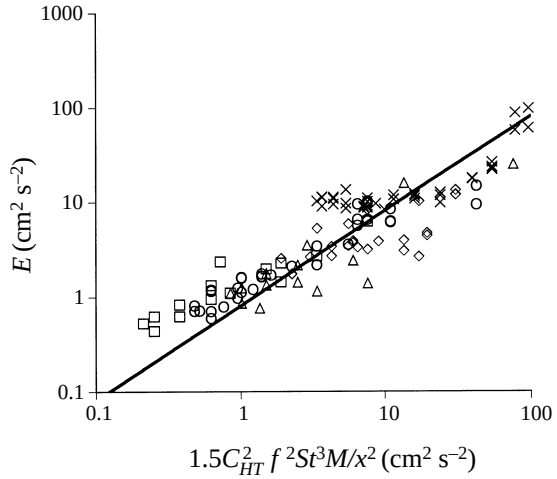

FIGURE 5. Comparison of the measured turbulent kinetic energy in the far field with the grid scaling relation for the turbulent kinetic energy (Hopfinger & Toly 1976). For the experiments, $St = 4$ cm and $f = 2$ Hz (squares), 3 Hz (circles), 4 Hz (triangles), 6 Hz (diamonds) and 8 Hz (crosses).

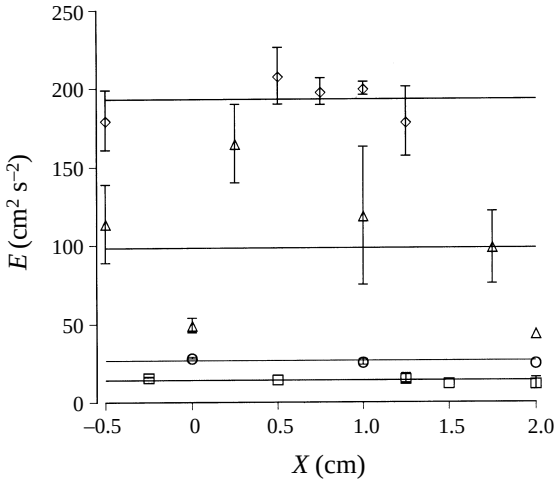

FIGURE 6. Spatial distribution of turbulent kinetic energy in the grid region when $St = 4$ cm and $f = 3$ Hz (squares), 4 Hz (circles), 6 Hz (triangles) and 8 Hz (diamonds). The horizontal lines are averages for each grid frequency and the error bars are $\pm$ one standard deviation from the mean when available.

Figure 6 summarizes the near-field results obtained by plotting the measured E versus distance from the oscillating grid centre for frequencies ranging from 3 to 8 Hz. The error bars are standard deviations from independent experiments when available. The turbulent intensity displayed no systematic dependence on position for distances less than 2 cm and therefore the near field was represented as a constant value, shown by the solid horizontal lines in figure 6. A plot of the average turbulent kinetic energy in the near field versus grid frequency (figure 7) exhibits the expected f^2 dependence. The symbols are averages of the E measurements made in the oscillating grid region at each frequency and the error bars represent 95 % confidence intervals. The correlation, $E = 2.93f^2$, fit the data with an $r^2 = 99\,\%$. Here, E has units of cm^2 s^{-2} and f is in Hz.

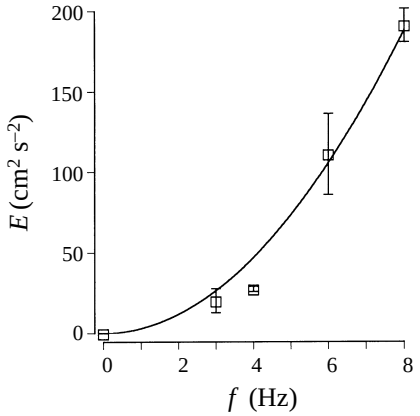

FIGURE 7. The average turbulent kinetic energy in the grid region versus the grid frequency. The solid line is a best-fit to the experimental data and error bars are 95% confidence intervals.

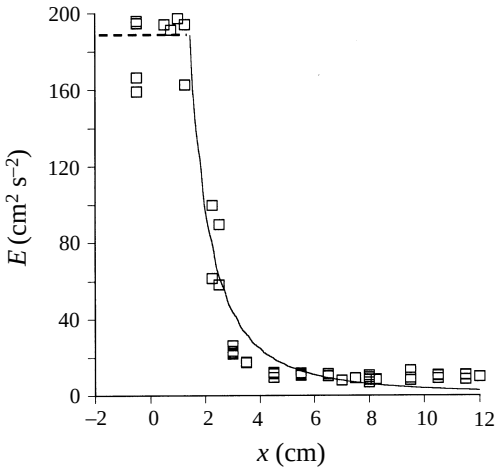

FIGURE 8. The spatial distribution of turbulent kinetic energy (E) as a function of horizontal distance from the oscillating grid. Results are shown for $St = 4$ cm and $f = 8$ Hz. The solid line represents the expected far field E-distribution and the dashed line is an average of the measurements made in the oscillating grid region.

The turbulent kinetic energy scaling relations valid for the inner and outer regions were combined to form a piecewise continuous approximation to the experimental data. The calculated E profile obtained for $f = 8$ Hz is shown in figure 8 along with the experimental data. At distances greater than about 1.45 cm from the grid, the turbulence followed the Hopfinger & Toly (1976) decay law shown as the solid line. Near the grid, turbulence intensity was assumed to be constant as illustrated with the dashed line in figure 8.

The average Kolmogorov shear rate at each operating condition was computed by taking the volumetric average of the measured Γ distributions assuming homogeneity in planes perpendicular to the grid motion as indicated by (5.5). Table 1 lists the computed spatially averaged Kolmogorov shear rates, $\langle\Gamma\rangle$, which range from 3.7 s^{-1} at $f = 1$ Hz to 83.6 s^{-1} at $f = 8$ Hz. The average Kolmogorov length scale varied from 520 to 109 μm as the grid frequency was changed from 1 to 8 hz. The estimate for η in the most turbulent regions of the tank ($x = 0$ cm) was found always to be above 50 μm

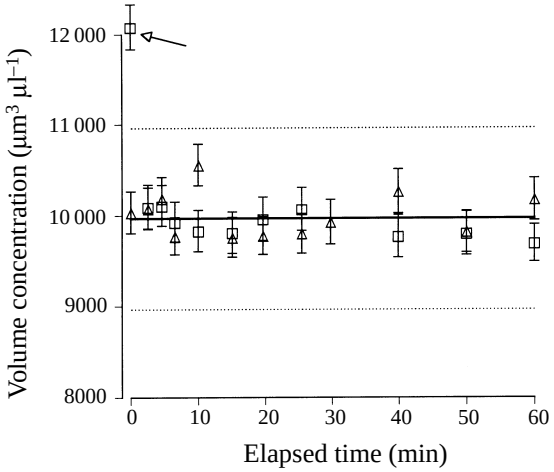

FIGURE 9. Volume concentration of particles as a function of time for a turbulent coagulation experiment when the grid was oscillating at 6 Hz. Shown are symbols for the two sampling positions. The solid line is the time-average volume concentration and the error bars are 95% confidence intervals based on Poisson statistics. The dashed lines demarcate $\pm 10\%$ of the mean and were used to identify data (marked with the arrow) inadvertently collected before the reactor was completely mixed.

(see table 1); therefore, the assumption that the particle diameters (3.9 μm) were much smaller than the Kolmogorov length scale applied for all the operating conditions used in the coagulation experiments.

5.3. *Analysis of turbulent coagulation measurements*

Turbulent coagulation experiments were conducted using the procedure outlined in § 3. From four to six independent experiments were performed for grid frequencies of 0, 1, 3, 4, 6 and 8 Hz. Figure 9 shows the mass balance as a function of time for an experiment conducted at $f = 6$ Hz. Shown are symbols for the two sampling ports as well as a solid line indicating the average mass in the system and dashed lines denoting $\pm 10\%$ of the mean. The error bars show 95% confidence intervals in the calculated concentrations based on Poisson statistics. Particle losses were not observed over the lifetime of the experiment and no statistically significant trend with sampling port was observed. These conditions also hold for the other turbulent coagulation experiments reported here. In addition, this mass balance illustrates how incomplete mixing was detected during an experiment. The $\pm 10\%$ boundaries were used to flag outlying samples exhibiting incomplete mixing and the aberrant samples were removed from the analysis. In the experiment depicted in figure 9, the first sample taken (marked with the arrow) had an abnormally high concentration indicative of incomplete mixing in the reactor and it was dropped from further analysis.

The evolution of the singlet concentration for the same $f = 6$ Hz experiment is plotted in figure 10. Shown are different symbols for the two sample ports. The error bars denote 95% confidence intervals based on Poisson statistics. The incomplete mixing point tagged using figure 9 is marked with an arrow on figure 10. The solid line is a regression through the data using the explicit breakup model, (3.6), in the region where triplet formation was negligible.

When we ran a coagulation experiment for a long time we observed that the particle size distribution reached a steady state (see the experimental results in figure 9)

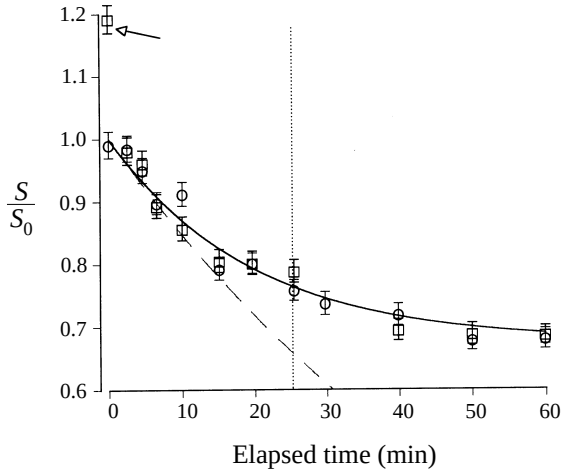

FIGURE 10. Coagulation rate data plotted for an experiment conducted with $f = 6$ Hz. Nonlinear regression using the integral rate expression with breakup (solid line) was used to estimate the coagulation rate constant. The dashed line is the expected behaviour if breakup is neglected. The symbols represent the two sample ports and error bars are 95% confidence intervals based on Poisson statistics. Data to the right of the vertical dotted line were expected to have significant triplet formation based on (3.4) and was not included in the regression. The arrow marks the data collected before mixing was complete.

where the number of singlet particles in the system remained nearly constant. This steady state could only be achieved by considering particle breakup – if aggregation were irreversible then the equilibrium state would be a single aggregate composed of all the singlet particles.

The importance of particle breakup may be seen by comparing the model prediction that includes particle breakup with the prediction obtained when break up is neglected, (3.2). The dashed line in figure 10 shows the model prediction when breakup is ignored. It can be seen that breakup is manifested by a deviation from the model prediction that neglects breakup (dashed line) at times greater than about 20 min.

Triplet formation was considered significant when the triplet formation rate was calculated to be greater than 20% of the doublet formation rate. Equation (3.4) shows that triplet formation became significant for $S/S_0 < 0.78$. This corresponded to data taken after 25 min and the boundary for significant triplet formation is shown by the vertical dotted line in figure 10. When triplet formation is significant, the singlet concentration should decrease faster than the model predictions based on doublet formation alone. The data in figure 10 do not show a deviation from the model prediction that ignores triplet formation – in fact, the effect of triplet formation was not observed for any of the experiments conducted. Since breakup would be expected to affect triplets more than doublets, perhaps it was instrumental in keeping the number of triplets in the system low. The nonlinear regression led to an estimate of $k_T = 431\ \mu\text{m}^3\ \text{s}^{-1}$.

A summary of the flocculation rate data obtained is shown in figure 11, where the coagulation rate constant is plotted against average Kolmogorov shear rate. The symbols represent the average of independent experiments (four to six runs for each grid frequency) and the error bars show 95% confidence intervals. A power law fit of the data (not shown in figure 11) indicates that $k_T = 2.1a^3\Gamma^{0.84}$ with an r^2 of 99.9%. Here the units on Γ are s^{-1}.

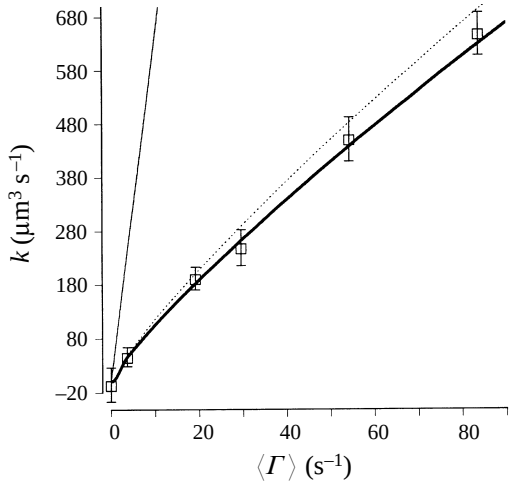

FIGURE 11. Summary of the experimentally determined coagulation rate constant as a function of average Kolmogorov shear rate. Shown are the averages with 95% confidence intervals for experiments conducted at several grid frequencies. The thin line is the prediction obtained when interparticle interactions are not included. Including van der Waals attraction and hydrodynamic interactions leads to the model prediction shown by the thick solid line when the coagulation rate constant is obtained by averaging over the local coagulation rates in the reactor. When the predicted coagulation rate is calculated using the average Kolmogorov shear rate, the curve presented as the dotted line results.

The analysis of the experimental data given in §3 assumes that the effect of Brownian coagulation is negligible. Péclet numbers based upon the Kolmogorov scales and the particle radius (shown in table 1) are larger than 79 for all turbulent coagulation experiments, suggesting that Brownian motion did not influence the results. However, Feke & Schowalter (1983, 1985) have shown that Brownian motion can affect the coagulation rate in simple shear or uniaxial extension at *Pe* values of 150 or higher. In steady flows at infinite *Pe*, large concentration gradients develop at the boundaries between streamlines that lead to coagulation and those that do not. Therefore, even at large *Pe*, Brownian motion allows particles to diffuse across these boundaries, thus measurably affecting the predicted coagulation rate (Feke & Schowalter 1983). In contrast, for a temporally varying linear flow, large concentration gradients do not persist because the fluctuating motion of the fluid acts to disperse particles. From a theoretical calculation of coagulation in a randomly varying flow field with small total strain, we found that Brownian motion was unimportant for *Pe* values much beyond 1 (Brunk *et al.* 1997). Turbulence has an intermediate total strain; thus, Brownian motion can be anticipated to be more important than predicted at the small total strain limit but less important than the analysis of Feke & Schowalter (1983) suggests. Although the effects of Brownian motion for isotropic turbulence have not been explicitly modelled, the excellent agreement between the model simulations and experiments (to be discussed below) suggests the influence of Brownian diffusion was insignificant for the Péclet numbers used in these coagulation experiments.

5.4. *Comparison with model predictions*

The thin solid line in figure 11 is the predicted coagulation rate based on the model simulations (2.8) described in §2 for non-interacting particles ($\alpha_T = 1$). Comparing the experimental data in figure 11 with the thin solid lines shows that the actual coagulation rate increases more slowly with shear rate than predicted by the non-

interacting particle model. The results that neglect particle interactions consistently overestimated the actual rate of coagulation and the error was exacerbated at larger shear rates because of differences in the power law dependence of k on $\langle\Gamma\rangle$.

Predictions based on the model calculations that include interparticle interactions are shown in figure 11 as the thick solid line. The computer simulations predict $k_T = 2.05a^3\langle\Gamma\rangle^{0.84}$, in close agreement with the best fit of the experimental data and yielding only a slightly lower $r^2 = 99.8\,\%$. It should be emphasized that no fitting parameters were used in this model prediction and, as described previously, estimates for the Hamaker constant and spatial Kolmogorov shear rate distribution were obtained in independent experiments.

We caution that the model predictions relating the coagulation rate constant to the spatially averaged Kolmogorov shear rate are system specific. Although the predicted power law dependence on Γ should remain the same, the pre-exponential factor will depend on the spatial distribution of turbulence within a particular system. The model prediction shown as the thick solid line on figure 11 was obtained by spatially averaging the turbulent coagulation rate constant, i.e.

$$\langle k_T\rangle = \frac{1}{20\text{ cm}}\int_{-4\text{ cm}}^{16\text{ cm}} k_T(\Gamma(x))\,\mathrm{d}x, \tag{5.6}$$

where spatial homogeneity in the plane perpendicular to the grid motion was assumed, $k_T(\Gamma)$ was given by (2.5) and $\alpha(\Gamma)$ in (2.5) was given by (2.6). Based on (5.6) and the measured Γ distribution, approximately 45 % of the total coagulation occurred in the far-field regions of the tank.

To illustrate the importance of accounting for local variations in Γ throughout the reactor, consider the proposal to characterize the turbulence with the average Kolmogorov velocity gradient: $\langle\Gamma\rangle$. The model prediction based upon $k_T(\langle\Gamma\rangle)$, shown as the dotted line on figure 11, overestimated the experimentally measured coagulation rate constants by about 11 %.

The experimental verification of the computer simulations relies on several parameters some of which have only been roughly measured in our research or taken from literature values. An examination of the model equations shows that there are four parameters that influence the model predictions, namely: B (proportionality constant relating distance from the oscillating grid to the integral length scale of turbulence), γ (proportionality constant relating the turbulent dissipation rate to the integral scales of velocity and length, see equation (5.2)), C_{HT} (proportionality constant relating the integral velocity to oscillating grid parameters, see equation (5.4)) and A_H (the Hamaker constant, a parameter in N_S defined in equation (2.6)).

B and γ are parameters of the turbulence that were not measured in this research and C_{HT} was measured with a high degree of accuracy. We can make two observations regarding the effects of these parameters on the model predictions for the coagulation rates: (i) the power law dependence of the aggregation rate with the Kolmogorov shear rate is independent of the values of B, γ and C_{HT}. The fact that both the model predictions and the experiments have the same power law dependence supports our conclusion that the model is accurately representing the turbulent shear aggregation rate. (ii) The model results are relatively insensitive to changes in the values of these parameters. We used the often cited value of $\gamma = 0.8$ from Townsend (1976). According to Fernando & Long (1985), other estimates for γ are lower than 0.8. For their study of density stratification in grid-generated turbulence, Fernando & Long (1985) chose $\gamma = 0.63$. Uncertainty analysis shows that decreasing γ by 0.2 decreases the predicted coagulation rate by 11 %. Published values for B range from 0.1 to 0.35

$\langle \Lambda \rangle$ (s^{-1})	k_T^{exp} ($\mu m^3\ s^{-1}$)	k_T^{pred} ($\mu m^3\ s^{-1}$)	Difference (%)	k_T^0 ($\mu m^3\ s^{-1}$)
89	4.9 ± 1.2	6.8	37	20.7
221	11.9 ± 3.0	14.5	22	51.4
377	17.7 ± 4.4	22.7	28	87.7

TABLE 2. Comparison of model prediction with the turbulent coagulation data collected by Delichatsios & Probstein (1975) in pipe flow. Model prediction uses the Hamaker constant obtained in this work and assumes a constant Kolmogorov shear rate in the turbulent pipe. Superscripts in the table stand for experimental measurements (exp), model prediction with interparticle forces (pred) and model prediction for non-interacting particles (0). The uncertainty interval in the experimental data corresponds to a 25% coefficient of variation using data summarized for the $\Gamma = 221\ s^{-1}$ data set.

(Hopfinger & Toly 1976) – decreasing B by a factor of 4 increases the coagulation rate by about 4%. The small measurement uncertainty in C_{HT} had a negligible impact on the coagulation rate.

The Hamaker constant, A_H, characterizes the strength of van der Waals attraction. It was measured using independent Brownian coagulation experiments. Our estimate was $0.75\ k_b T$ with 60% confidence intervals of $0.5 k_b T$ to $1.3 k_b T$. It is possible to show that doubling the Hamaker constant increases the model prediction by 12%. We conclude that the errors associated with our estimates for these four parameters only weakly affect the model predictions and do not affect the exponent in the power law relationship between the coagulation rate constant and the spatially averaged Kolmogorov shear rate.

The only turbulent coagulation data by other investigators that are amenable to comparison with the computer simulations are those published by Delichatsios & Probstein (1975). These investigators measured the coagulation rate of 0.6 μm diameter polystyrene particles in turbulent pipe flow having Reynolds numbers ranging from 15000 to 50000 based upon the pipe diameter and mean velocity. A summary of their results and a comparison to our model predictions is shown in table 2. Average Kolmogorov shear rates ranged from 89 s^{-1} to 377 s^{-1} and measured coagulation rate constants varied from 4.9 $\mu m^3\ s^{-1}$ to 17.7 $\mu m^3\ s^{-1}$ for the most destabilized systems reported. Error bars provided for the $\Gamma = 221\ s^{-1}$ experiments indicate a coefficient of variation of about 25% and the same relative error was assumed for the other two experimental conditions.

Estimates of the coagulation rate assuming non-interacting particles overestimate the coagulation rates observed by Delichatsios & Probstein (1975) by factors of four to five. The model predictions using the Hamaker constant found in this work and an extrapolation of (2.6) to 0.6 μm diameter particles overestimated the coagulation rate by 22% to 37% when the average Kolmogorov shear rate in the core region was used to characterize the turbulence within the pipe. This model prediction is considerably better than estimates based on non-interacting particles and deviations from the experiments can at least partly be explained by experimental accuracy. The trend of the experimental data was well represented by a power law correlation of the form: $k = 4.52 a^3 \Gamma^{0.84}$ ($r^2 = 99.5\%$), where the units of Γ are s^{-1}. Thus, the turbulent pipe experimental coagulation data show the same power law trend as that predicted by the computer simulations. The Péclet numbers of the turbulent pipe flow experiments were five to 23, about an order of magnitude lower than the Pe for the experiments reported in this paper. Therefore, it is likely that Brownian diffusion affected the results of Delichatsios & Probstein's work. Brownian motion increased the coagulation rate in

Feke & Schowalter's (1984) analysis of simple shear coagulation and in our pair diffusion approximation for coagulation in a random linear flow (Brunk *et al.* 1997). This expectation is in opposition to the discrepancy between the experimental data of Delichatsios & Probstein and the non-Brownian model predictions presented in table 2. The spatial variation of turbulent shear rates in the pipe flow was ignored in the analysis of Delichatsios & Probstein's experimental data and this could be an additional source of error between experiment and simulation. For grid-stirred turbulence, the constant Kolmogorov shear rate approximation led to model predictions that overestimated the experimental results. Except very near the pipe wall, turbulence in pipe flow is nearly homogeneous (Delichatsios & Probstein 1975). While it is likely that spatial heterogeneities in the turbulent shear rates caused some of the error in the model predictions for Delichatsios & Probstein's coagulation experiments, preliminary analysis suggests that the relatively small turbulent boundary layer in pipe flow is unlikely to drastically alter the model prediction summarized in table 2. Particle breakup due to the high Kolmogorov shear rates in the pipe flow are another possible cause for the differences between the model and experimental data of Delichatsios & Probstein (1975). An inspection of the experimental singlet evolution data in the turbulent pipe flow coagulation experiments does not show deviations from linearity, indicating the breakup was probably unimportant. In the light of these concerns, the simulations with interparticle forces reproduce the coagulation experiments conducted by Delichatsios & Probstein (1975) remarkably well and are able to predict the correct dependence on Kolmogorov shear rate.

6. Summary and conclusions

Experimental measurements of turbulent coagulation were compared with model predictions that included viscous effects and van der Waals attraction. An initially monodisperse suspension of 3.9 μm diameter polystyrene beads was placed in the reactor and the loss of singlets over time was measured as a function of turbulence intensity in the reactor. The particles were smaller than the Kolmogorov length scale so that turbulent shear rates at the Kolmogorov scale controlled the coagulation rate while differential settling and particle inertia effects were minimized by running the experiments in density-matched fluids.

An oscillating grid reactor system was purposely chosen for these experiments because grid-stirred devices produce well characterized, nearly isotropic turbulence that decays rapidly with distance from the oscillating grid. Considerable effort was expended to measure the spatial distribution of turbulence within the reactor so the experimentally observed average coagulation rate constant could be related to an average of the local coagulation within the reactor. Grid scaling laws developed and verified by others (Hopfinger & Toly 1976; De Silva & Fernando 1992; Brumley & Jirka 1987; Fernando & Long 1988) were found to represent the turbulent kinetic energy at distances greater than about $2M$ from the oscillating grid. Within the grid region ($x < 2$ cm), the turbulent kinetic energy showed no systematic variations with position and was, therefore, represented as a constant. A scaling law was used to relate the measured E-profiles to the dissipation rate in the reactor and then through Kolmogorov's similarity hypothesis to the Kolmogorov shear rate, Γ.

It is difficult to develop an experimental system for measuring particle aggregation in turbulent flows in which both the particle properties and the fluid dynamics can be sufficiently characterized. The high cost of monodisperse particles means the system must invariably be closed. By necessity, in a closed system the particles will interact

with the turbulence-generating mechanism – meaning the particles will sample regions of high-shear inhomogeneous turbulence. To our knowledge, no previous experimental studies of turbulent coagulation have attempted to address the fluid dynamics to the extent provided within this manuscript.

The experimental coagulation rate constant was found to be proportional to $\langle \Gamma \rangle^{0.84}$, in agreement with the model predictions. For comparison, analytical (such as Saffman & Turner 1956 or Brunk *et al.* 1997) and model (Brunk *et al.* 1998) predictions that neglect particle interactions suggest that $k \propto \Gamma$. These results, summarized in figure 11, indicate that interparticle interactions play an important role in controlling the rate of turbulent coagulation. Model predictions incorporating particle interactions were obtained by averaging over the local coagulation rate constants in the reactor. These simulation results agreed with experiment ($r^2 = 99.8\,\%$) without use of adjustable parameters. The spatial variation of turbulence within a coagulating system was shown to influence the model prediction. For instance, characterizing the turbulence in the tank with $\langle \Gamma \rangle$ led to a prediction that overestimated the experimental data by 11 %.

Comparison of the model and experimental turbulent coagulation rate constant predictions required knowledge of the Hamaker constant for the coagulating polystyrene beads. The Hamaker constant was obtained through Brownian coagulation experiments. A Hamaker constant of $0.75 k_b T$, consistent with other investigations (Russel *et al.* 1989), resulted in agreement between the experimental and theoretical Brownian coagulation rate.

To the authors' knowledge, no previous attempt has been made to quantify the importance of particle interactions in turbulent coagulation of interacting particles, either theoretically or experimentally. Numerous studies have, however, been conducted for steady linear flows (see Green, Hammer & Olbricht 1994 for a review of past work). Trajectory calculations for coagulation in simple shear and uniaxial extension that include hydrodynamic and van der Waals forces show a similar dependence on the shear rate as that obtained in this paper. Feke & Schowalter (1983) found that $k \propto \Gamma^{0.77}$ for simple shear and Zeichner & Schowalter (1977) obtained $k \propto \Gamma^{0.89}$ for uniaxial extension; both are similar to the $k \propto \Gamma^{0.84}$ dependence measured for turbulent coagulation in this work.

Considerable empirical evidence garnered from flocculation studies of natural sediments indicates that collision efficiencies near 10 % are typical for destabilized colloidal particles (O'Melia 1995). The turbulent shear rates and particle sizes used in this research are within the range of typical values expected for natural aquatic environments such as estuaries (Krone 1970; McCave 1984) and so collision efficiencies calculated for the data reported here are amenable to comparison with field measurements. The collision efficiency for the experimental data in figure 11 can be estimated by dividing the flocculation rate obtained experimentally with that predicted by the non-interacting model given by (2.5) with $\alpha_T = 1$. The calculated collision efficiencies fall from 15 % at the low shear rates to 9 % at the highest shear rate examined in these experiments, in qualitative agreement with field measurements (O'Melia 1995).

The similarity of the theoretical predictions and the experimental measurements is remarkable considering the expected errors associated with using scaling arguments to calculate Γ and the use of several experimentally derived constants. While the absolute values of the Kolmogorov shear rate in the reactor may be suspect, the predicted $k \propto \langle \Gamma \rangle^{0.84}$ power law remains robust. The fact that both experiments and model simulations have the same power law dependence leads us to conclude that the computer simulations of coagulation in isotropic turbulence at finite total strain

(Brunk *et al*. 1998) capture the essential physics of turbulent coagulation. For neutrally buoyant particles with diameters smaller than the length scales of turbulence, the rate of coagulation is dominated by the Kolmogorov scales of turbulence. Relative particle motion on length scales comparable to the particle radius is the rate-limiting step for turbulent shear coagulation and consideration of particle interactions is necessary to explain experimental observations. Since isotropy at the small scales is universally seen for turbulent flows, the turbulent coagulation simulations validated in this manuscript should have wide application to other engineered and naturally occurring turbulent systems.

This research was sponsored by ONR (Contract N00014-94-1-0896) with additional funding provided by DoD's Air Force fellowship program. The authors thank Damaris Santos for her work on coagulation of polystyrene beads while visiting Cornell University under an NSF Research Experience for Undergraduates fellowship. We thank Anna Jensen, Dr Gerhard Jirka and Dr Monroe Weber-Shirk for their beneficial discussions. Additionally, Cameron Willkens and Lee Virtue are thanked for their assistance with the maintenance of the equipment used in these experiments.

REFERENCES

Appiah, A. & O'Melia, C. R. 1990 *Coagulation Processes: Destabilization, Mixing and Flocculation* in *Water Quality and Treatment*. *Pontius* (ed. W. Frederick). McGraw-Hill.

Atkinson, J. F., Damiani, L. & Harleman, D. R. F. 1987 A comparison of velocity measurements using a laser anemometer and a hot-film probe, with applications to grid-stirring entertainment experiments. *Phys. Fluids* **30**, 3290.

Batchelor, G. K. 1976 Brownian diffusion of particles with hydrodynamic interactions. *J. Fluid Mech*. **74**, 1.

Brumley, B. H. & Jirka, G. H. 1987 Near-surface turbulence in a grid-stirred tank. *J. Fluid Mech*. **183**, 235.

Brunk, B. K., Koch, D. L. & Lion, L. W. 1997 Hydrodynamic pair diffusion in isotropic random velocity fields with application to turbulent coagulation. *Phys. Fluids* **9**, 2670–2691.

Brunk, B. K., Koch, D. L. & Lion, L. W. 1998 Turbulent coagulation of colloidal particles. *J. Fluid Mech*. **364**, 81–113.

Brunk, B., Weber-Shirk, M., Jensen, A., Jirka, G. & Lion, L. W. 1996 Modeling natural hydrodynamic systems with a differential-turbulence column. *J. Hydraul. Engng* **122**, 373–380.

Camp, T. R. & Stein, P. C. 1943 Velocity gradients and internal work in fluid motion. *J. Boston Soc. Civil Engng* **30**, 219–237.

Casson, L. W. & Lawler, D. F. 1990 Flocculation in turbulent flow: measurement and modeling of particle size distributions. *AWWA J*. **8**, 54–68.

Clark, M. M. 1985 Critique of Camp and Stein's RMS velocity gradient. *J. Environ. Engng* **222**, 741–754.

Delichatsios, M. A. & Probstein, R. F. 1975 Coagulation in turbulent flow: theory and experiment. *J. Colloid Interface Sci*. **51**, 394–405.

De Silva, I. P. D. & Fernando, H. J. S. 1992 Some aspects on mixing in a stratified turbulent patch. *J. Fluid Mech*. **240**, 601.

E, X. & Hopfinger, E. J. 1986 On mixing across an interface in stably stratified fluid. *J. Fluid Mech*. **166**, 227.

Elimelech, M., Gregory, J., Jia, X. & Williams, R. 1995 *Particle Deposition and Aggregation Measurement Modeling and Simulation*, pp. 180–188. Butterworth-Heinemann.

Feke, D. L. & Schowalter, W. R. 1983 The effect of Brownian diffusion on shear-induced coagulation of colloidal dispersions. *J. Fluid Mech*. **133**, 17–35.

Feke, D. L. & Schowalter, W. R. 1985 The influence of Brownian diffusion on binary flow-induced collision rates in colloidal dispersions. *J. Colloid Interface Sci*. **106**, 203–214.

FERNANDO, H. J. S. & LONG, R. R. 1985 On the nature of the entrainment interface of a two-layer fluid subjected to zero-mean-shear turbulence. *J. Fluid Mech.* **151**, 21.

GIBBS, R. J. 1982 Floc stability during Coulter-Counter size analysis. *J. Sediment. Petrol.* **52**, 657–660.

GIRIMAJI, S. S. & POPE, S. B. 1990 A diffusion model for velocity gradients in turbulence. *Phys. Fluids* A **2**, 242–256.

GREENE, M. R., HAMMER, D. A. & OLBRICHT, W. L. 1994 The effect of hydrodynamic flow field on colloidal stability. *J. Colloid Interface Sci.* **167**, 232–246.

HOPFINGER, E. J. & TOLY, J. A. 1976 Spatially decaying turbulence and its relation to mixing across density interfaces. *J. Fluid Mech.* **78**, 155–175.

JENSEN, A. 1997 Experiments and modeling of turbulence, salinity and sediment concentration interactions in a simulated estuarine water column. MS Thesis. School of Civil & Environmental Engineering. Cornell University.

KIM, S. & KARRILA, S. J. 1991 *Microhydrodynamics: Principles and Selected Applications*. Butterworth-Heinemann.

KRONE, R. B. 1978 *Estuarine Transport Processes* (ed. B. Kferfve). University of South Carolina Press.

LOHRMAN, A., CABRERA, R. & KRAUS, N. C. 1994 *Proc. Symp. on Fundamentals and Advancements in Hydrodynamic Measurements and Experimentation* (ed. C. A. Pugh), p. 351. ASCE.

MCCAVE, I. N. 1984 Size spectra and aggregation of suspended particles in the deep ocean. *Deep-Sea Res.* **31**, 329–352.

O'MELIA, C. R. 1980 Aquasols: the behavior of small particles in aquatic systems. *Environ. Sci. Technol.* **14**, 1052–1060.

O'MELIA, C. R. 1995 *From Algae to Aquifers* in *Aquatic Chemistry Interfacial and Interspecies Processes* (ed. C. P. Huang, C. R. O'Melia & J. J. Morgan). ACS, Washington, DC.

PEARSON, H. J., VALIOULIS, I. A. & LIST, E. J. 1984 Monte Carlo simulation of coagulation in discrete particle-size distributions. Part 1. Brownian motion and fluid shearing. *J. Fluid Mech.* **143**, 367.

POPE, S. B. 1990 Lagrangian microscales of turbulence. *Phil. Trans. R. Soc. Lond.* **333**, 309–319.

PRESS, W. H., TEUKOLSKY, S. A., VETTERLING, W. T. & FLANNERY, B. P. 1992 *Numerical Recipes in C*. Cambridge University Press.

RUSSEL, W. B., SAVILLE, D. A. & SCHOWALTER, W. R. 1989 *Colloidal Dispersions*. Cambridge University Press.

SAFFMAN, P. G. & TURNER, J. S. 1956 On the collision of drops in turbulent clouds. *J. Fluid Mech.* **1**, 16–30.

SCHENKEL, J. H. & KITCHENER, J. A. 1960 A test of the Derjaguin–Verwey–Overbeek theory with a colloidal suspension. *Trans. Faraday Soc.* **56**, 161.

SPIELMAN, L. A. 1970 Viscous interactions in Brownian coagulation. *J. Colloid Interface Sci.* **33**, 562–571.

STUMM, W. & MORGAN, J. J. 1981 *Aquatic Chemistry: An Introduction Emphasizing Chemical Equilibrium in Natural Waters*. Wiley.

TENNEKES, H. & LUMLEY, J. L. 1972 *A First Course in Turbulence*. MIT Press.

TOWNSEND, A. A. 1976 *The Structure of Turbulent Shear Flow*, 2nd Edn. Cambridge University Press.

VALIOULIS, I. A. & LIST, E. J. 1984 Collision efficiencies of diffusing spherical particles: hydrodynamic, van der Waals and electrostatic forces. *Adv. Colloid Interface Sci.* **20**, 1.

ZEICHNER, G. R. & SCHOWALTER, W. R. 1977 Use of trajectory analysis to study stability of colloidal dispersions in flow fields. *AIChE J.* **23**, 243–254.